Detection of single ions in a nanoparticle coupled to a fiber cavity

Chetan Deshmukh,[1,†] Eduardo Beattie,[1,†] Bernardo Casabone,[1] Samuele Grandi,[1,*]
Diana Serrano,[2] Alban Ferrier,[2,3] Philippe Goldner,[2] David Hunger,[4,5] and
Hugues de Riedmatten[1,6]

[1]ICFO-Institut de Ciencies Fotoniques, The Barcelona Institute of Science and Technology, 08860 Castelldefels (Barcelona), Spain
[2]Chimie ParisTech, PSL University, CNRS, Institut de Recherche de Chimie Paris, Paris, France
[3]Faculté des Sciences et Ingénierie, Sorbonne Université, UFR 933, 75005 Paris, France
[4]Karlsruher Institut für Technologie, Physikalisches Institut, Karlsruhe, Germany
[5]Karlsruhe Insitute for Technology, Institute for Quantum Materials and Technologies (IQMT), Eggenstein-Leopoldshafen, Germany
[6]ICREA-Institució Catalana de Recerca i Estudis Avançats, 08015 Barcelona, Spain
[†]These authors contributed equally to this work.
*samuele.grandi@icfo.eu

Many quantum information protocols require the storage and manipulation of information over long times, and its exchange between nodes of a quantum network across long distances. Implementing these protocols requires an advanced quantum hardware, featuring, for example, a register of long-lived and interacting qubits with an efficient optical interface in the telecommunication band. Here we present the Purcell-enhanced detection of single solid-state ions in erbium-doped nanoparticles placed in a fiber cavity, emitting photons at 1536 nm. The open-access design of the cavity allows for complete tunability in both space and frequency, selecting individual particles and ions. The ions are confined in a volume two orders of magnitude smaller than in previous realizations, increasing the probability of finding ions separated by only a few nanometers, which could then interact. We report the detection of individual spectral features presenting saturation of the emission count rate and linewidth, as expected for two-level systems. We also report an uncorrected $g^{(2)}(0)$ of 0.24(5) for the emitted field, confirming the presence of a single emitter. Our fully fiber-integrated system is an important step towards the realization of the initially envisioned quantum hardware.

1. INTRODUCTION

The basic constituent element of a distributed quantum computing system has to be able to address and manipulate qubits with long lifetimes and interface them with other computing centers over a quantum network. Such a critical enabling system would likely entail the use of spin–photon interfaces [1], which allow for the manipulation of long-lived matter qubits and their mapping to photons for long-distance information transfer with low loss. This route has been extensively researched, with systems ranging from the laser trapping of single atoms and ions [2–4] to solid-state systems such as quantum dots [5] or color centers in solids [6,7].

To enhance the light–matter interaction and ensure an efficient collection of photons, a common approach is to change the local density of states around the emitter, e.g., by engineering photonic nanostructures [8,9] or by placing the matter qubit in a low-volume and high-finesse optical cavity [10]. The natural lifetime of the optical transition is reduced through the Purcell effect [11], and this reduction could eventually lead to lifetime-limited operation, despite the excess dephasing typical of solid-state systems. However, the modifications required for the inclusion of a high-finesse cavity often heavily burden other aspects, for example, limiting the maximum number of interconnected qubits or introducing additional decoherence channels due to the nanostructuring of the environment close to the emitters.

Rare-earth-ion-doped solids (REIDSs) in nanostructures provide a system that could benefit from high Purcell enhancement without critical reduction in coherence. REIDSs have been extensively used as a platform for light–matter interaction, providing an ensemble of atoms with long coherence times naturally trapped in a solid-state matrix [12], and they are a leading system for optical quantum memories [13–16] and quantum repeater applications [17–19]. Among the rare-earth ions, erbium offers direct operation at telecommunication wavelengths, as well as long optical [20] and spin coherence times [21] at low temperature and with suitable magnetic fields. Recently, efforts have been made to detect single ions, to facilitate the manipulation of individual spins. This approach enables long-lived and efficient spin–photon interfaces and quantum gates between single ion qubits by harnessing dipolar interactions, which opens the door to quantum processing nodes [22–24] with a high degree of connectivity both within each

node and between network nodes. For that application, the ions present in each node need to be spectrally distinguishable to allow individual addressing of all the ions. Quantum repeaters using single rare-earth-ion qubits have also been proposed, combining a processing ion with a long coherence time (e.g., europium [25,26] or praseodymium [27]) and a communication erbium ion at telecommunication wavelength [28]. Following early experiments in free space [29,30], single rare-earth ions coupled to cavities have emerged as a powerful platform enabling single ion detection and manipulation [31,32], single shot readout [33,34], addressing of several qubits in the spectral domain [35,36], fast modulation of cavity coupling [37], coupling to long-lived nuclear spins [38,39], and generation of indistinguishable telecom photons [40].

Most of these experiments have been done with nanophotonic cavities where the interaction volume was comparable to the cavity mode volume and reached a minimum of order of $0.5\lambda^3$. In these conditions, the doping concentration has to remain small to limit the total number of ions such that most individual ones can be addressed. This makes it challenging to find several ions within a few nm distance, as required for performing dipolar gates [24]. Open-access microcavities have recently shown great promise, providing fast tuning and 3D positioning. They have been coupled to several solid-state emitters [36,41–44], improving light–matter interaction and photon collection efficiency.

Here we use a similar approach exploiting an open-access fiber microcavity and erbium-doped nanoparticles [45]. It combines the advantages of an open-access design with the high concentration of dopants and small volume available in nanoparticles, all in a fiber-integrated device able to select separate particles and spectrally tune to single solid-state emitters. All the ions are concentrated in a volume more than two orders of magnitude smaller than in previous realizations, due to the low volume of the nanoparticle that is much smaller than the mode of the cavity. We show that Purcell enhancement of up to 120 can be achieved in this setup, and we show clear signatures of single ion detection. Single spectral features are identified and investigated, and we report Zeeman splitting of an emission line in the presence of a magnetic field and saturation of the emitted fluorescence for increasing excitation power. Finally, for one of these features, we report a measurement

of the second-order auto-correlation function $g^{(2)}(\tau)$ of the collected fluorescence, with an uncorrected zero-delay value well below the limit of 0.5 for single emitters, and compatible with the one expected given the dark count rate of the detectors. The full experiment is run in a fiber-integrated fashion, with both excitation and detection performed through a telecom fiber, and is therefore suitable for long-distance quantum communication. Our system provides a fully fiber-coupled interface that could be adapted to other types of nanoparticles, from other rare-earth ions [46] to color centers [47] or dye molecules [48], or even to crystalline membranes, addressing a register of optically active solid-state spins.

2. DESCRIPTION OF THE SETUP

An outline of the setup is presented in Fig. 1. Our cavity is composed of a planar dielectric mirror, on which the nanoparticles are deposited, and a concave mirror on the tip of a single mode fiber. The latter is realized by first evaporating a spherical indentation on an optical fiber using a CO_2 laser, and then depositing a highly reflective dielectric coating over it [49]. The obtained mirror has a radius of curvature of 60 μm, which, considering a targeted cavity length of 6 μm, results in a cavity mode waist of 3 μm and a mode volume $V \approx 40$ μm^3, or about $10\lambda^3$. The cavity was designed to maximize the escape of photons towards the optical fiber through the curved fiber mirror, which has a transmittivity of 100 ppm versus the 30 ppm introduced by the planar mirror. The latter coating was additionally engineered to place an antinode of the electric field 50 nm above the surface of the planar mirror, therefore ensuring a maximum field enhancement at the position where nanoparticles are placed. Given these parameters, the empty cavity has an expected finesse of 44,000 at 1535 nm, a quality factor $Q \approx 10^5$, and a full-width at half-maximum (FWHM) of 600 MHz.

The cavity was assembled on a homemade nano-positioner placed inside a closed-cycle cryostat, with a design improved from our previous experiment [45]. It aims to reduce the mechanical noise of the closed-loop cryostat while at the same time cooling the nanoparticles on the planar mirror. The assembly allows for full 3D positioning of the fiber through the use of piezo-positioners that
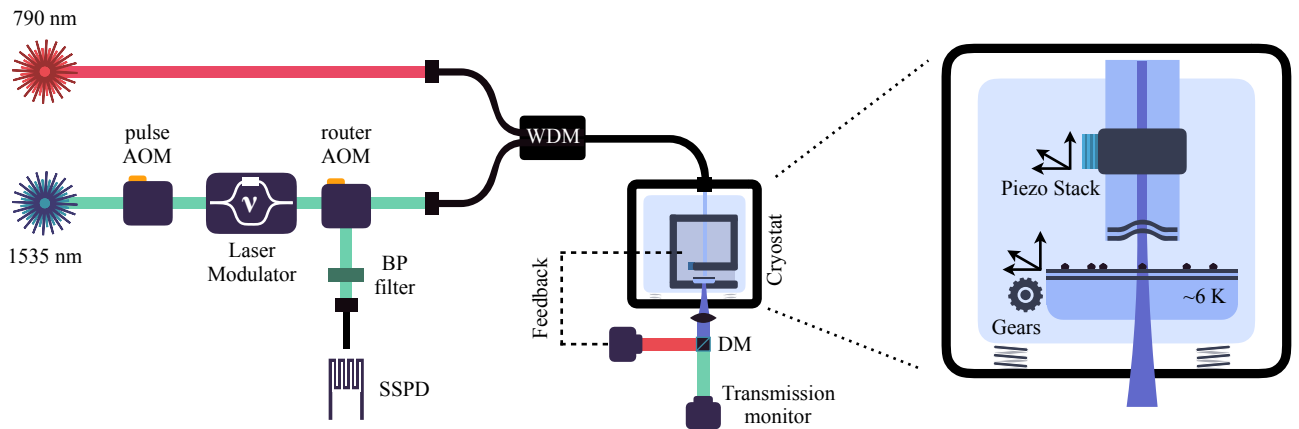
Fig. 1. Description of the setup. A laser at 1535 nm provides the excitation light for the erbium ions. The light is shaped into pulses by an acusto-optic modulator (AOM), and its frequency is further controlled using a modulator. The cavity is stabilized using a laser at 790 nm, which is combined with the excitation light through a wavelength-division multiplexer (WDM). The optical fiber is fed into the cryostat where the fiber cavity is placed. The transmission of the 790 nm laser through the cavity is monitored to stabilize the cavity length to 20 pm RMS. The fluorescence from the ions is collected back through the optical fiber and directed to superconducting detectors (SSPD) using a router AOM. Right: schematic of the fiber cavity setup. DM, dichroic mirror.

bend the arm that the fiber is attached to, and for coarse 3D scanning of the position of the planar mirror with three DC motors. This grants total freedom in the selection of the length of the cavity and of the region of the mirror that is analyzed, enabling the free selection of different nanoparticles and optical modes.

The nanoparticles are of Y_2O_3 and doped with a concentration of 20 ppm of erbium ions. They are single nanocrystals with a Gaussian size distribution centered at 110 nm with a sigma of 30 nm, corresponding to an average volume of $7 \cdot 10^{-4}$ μm^3 [26]. After synthesis, the nanoparticles are dispersed in ethanol, passed in a sonic bath to help separate aggregates of nanocrystals, and then deposited on the flat mirror through spin coating [50]. The mirror is then integrated with the fiber-cavity mount, where it is cooled to about 6.5 K. Figure 1 shows a schematic of the setup. The coating of the mirrors was further designed to provide a double resonance: at 1535 nm, corresponding to the erbium transition, and at 790 nm, which is used to lock the cavity using an additional laser. The cavity length is then stabilized to within 20 pm RMS when the cryostat is turned on, mostly limited by the additional mechanical vibrations introduced. This introduced a duty-cycle for our experiment of about 70%.

The ions are investigated by addressing the $^4I_{15/2} \leftrightarrow {}^4I_{13/2}$ transition at 1535 nm of the erbium ions in the C_2-symmetry site and detecting the fluorescence emitted in the cavity. The excitation light is provided by an external-cavity diode laser that is frequency-stabilized to a high-finesse ultra-stable reference cavity. The amplitude of the light is controlled through three double-pass acousto-optic modulators (AOMs). To scan the frequency over a large range with high frequency resolution and while maintaining the laser locked, we use a frequency modulator developed by Thales Research & Technology and based on an IQ modulator [51], which allows us to tune the frequency over a range of 3 GHz. With this system, we can then control the population of the ions on a time scale much smaller than their lifetime, which allows us to perform a pulsed excitation scheme with excitation and detection of the ions separated in time, removing unwanted fluorescence. Moreover, the signal-to-noise ratio can be increased by reducing the collection window to include only the first portion of the fluorescence exponential decay, at the cost of a reduced total count rate. During the course of the experiment, we used an excitation pulse of 200 µs and a detection window of 500 µs, for a repetition rate of 1.4 kHz. The fluorescence emitted by the ions is then collected in the fiber and directed to a superconducting single photon detector, with efficiency ~80% and dark count rate 8 Hz, via a router AOM switch and a narrowband spectral filter. The efficiency of the superconducting detectors can be reduced to achieve a lower dark count rate, resulting in a higher signal-to-noise ratio.

3. SINGLE ION DETECTION

Individual nanoparticles are located through scattering-loss microscopy using the fiber cavity, detecting the reduction in transmission that is introduced by the particle. A typical scan is shown in Fig. 2(a), showing dark spots where the nanoparticles are located. Suitable particles are chosen based on the loss that they introduce in the cavity, aiming for a minimum reduction in finesse to maintain a high Purcell factor. Fluorescence from the ions is detected through the cavity by first exciting the ions and then opening a detection path to single photon detectors using a router AOM [45]. Through fluorescence decay measurements, we verified the presence of erbium ions and measured decay constants ranging
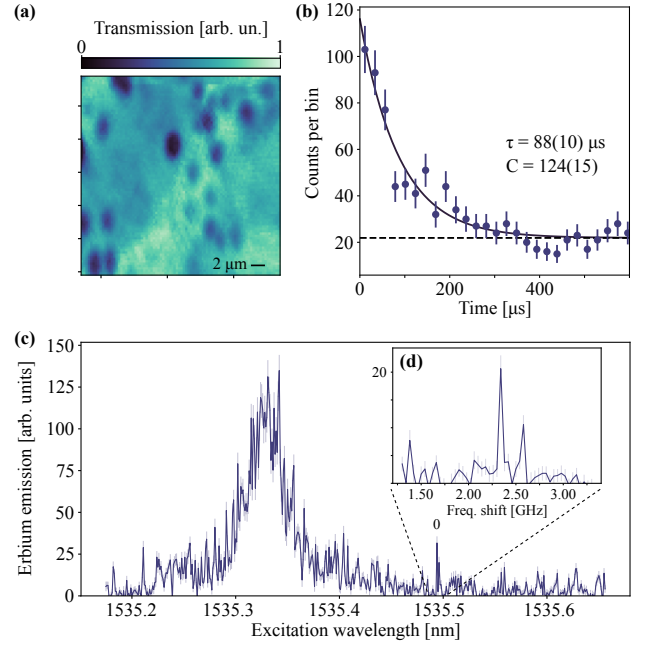
Fig. 2.　(a) Transmission microscopy image of several nanoparticles, identified by the reduction in cavity transmission. (b) Fluorescence decay measurement of an ensemble of erbium ions in a nanoparticle, showing Purcell enhancement of the lifetime. (c) Fluorescence scan of the inhomogeneous broadening of a nanoparticle, reporting the fluorescence photons collected as the excitation wavelength is changed. (d) Narrow fluorescence scan of the excitation frequency through the laser modulator, where an individual feature can be identified.

from one hundred to a few hundred microseconds. Individual values are affected by the orientation of the dipoles in the particle and by the stability of the cavity. Nevertheless, considering the natural lifetime of ~11 ms [45] and a minimum measured lifetime of 88(10) µs, reported in Fig. 2(b) for a small ensemble of ions, we were able to demonstrate a Purcell factor $C = 123(14)$. We can then give the ion–cavity coupling values of $\kappa = 2\pi \cdot 1.25$ GHz and $g = 2\pi \cdot 0.74$ MHz. The calculation of the expected Purcell factor requires a value of the branching ratio ζ of the investigated transition, for which only a lower bound of 0.13 has been measured so far [46]. Considering that the finesse of the cavity was reduced to about 20,000 while coupled to the particle, this would correspond to an expected Purcell factor

$$C_{\exp} = \zeta \frac{3\lambda^3}{4\pi^2} \frac{Q}{V} > 170,$$

which is close to our experimental results. Sub-optimal dipole orientation and cavity instability are among the parameters that could contribute to a reduction of the measured value.

The center and width of the inhomogeneous broadening of the $^4I_{15/2} \leftrightarrow {}^4I_{13/2}$ transition varies among the nanoparticles, and are determined by collecting the erbium fluorescence while performing a wide scan of the excitation light wavelength across several hundreds of pm. One such scan is shown in Fig. 2(c). For this nanoparticle, the width of the inhomogeneous broadening is 6 GHz, and from the reduction in transmission, we can estimate its diameter to be about ~170 nm [45,50], suggesting it is either a large nanocrystal or an aggregate of about two smaller ones. Given its size, an average of 1000 ions in the C2 site (75% of the total, based on the crystallographic structure of Y_2O_3 and on the similar

ionic radii of Er and Y [52]) can be investigated in this nanoparticle in the optical mode of the cavity. We can then deduce a spectral density of ~150 ions/GHz in the nanoparticle, in the center of the inhomogeneous line [27]. The ion density is 400×10^3 ions/μm^3. This value is several orders of magnitude higher than in similar systems [31,36], and of particular importance for the realization of two-qubit gates, for example, through ion–ion interaction [22,24].

Several individual spectral features can already be recognized in Fig. 2(c). Probing their single emitter nature further, we focused on their spectral linewidth. We observed features with widths ranging from 10 to 400 MHz. Considering the values of homogeneous linewidths in ensembles of nanoparticles measured at the current temperature [46], we would expect widths in the range of 4–10 MHz. However, we also expect that ions closer to the surface of the nanoparticles or close to lattice defects such as crystal boundaries would experience additional dephasing and therefore show wider lines. Some ions showed clear signs of spectral diffusion, ranging from a few seconds to a few minutes (see Supplement 1), which could also be compatible with an unfavorable positioning inside the nanoparticle.

We then turned to the full characterization of a narrow single spectral feature to confirm its single ion nature. We focused on the emitter indicated in Fig. 2(d), for which we measured lifetimes of 350–470 μs, depending on the specific cavity stability conditions (see Supplement 1), and corresponding to $g = 2\pi \cdot 0.35$ MHz and a Purcell factor of ≈ 30. The emitter showed stable emission, with a variable drift in the central excitation frequency at most comparable to its linewidth (see Supplement 1), and no significant long-term drift over more than two months. We investigated further, and by adding a small magnetic field with a permanent magnet ($\approx 10^2$ G), we were able to fully split the line, as visible in Fig. 3(a), consistent with the Zeeman splitting of a single erbium ion. The spectral linewidth measured for an excitation power of 220 pW decreases from ~30 to ~12 MHz when applying the magnetic field, which may be due to the presence of a spurious field weakly splitting the levels even when no external field is applied. We then selected one of these lines and performed fluorescence excitation measurements for increasing P, recording the probability of detection p_{det} of a photon at the center of the excitation line and its linewidth. One such scan is shown in Fig. 3(b), with a linewidth of 3.8 MHz obtained at $P = 22$ pW. We observed saturation of the fluorescence counts compatible with a single ion, as shown in Fig. 3(c). The first set of data is well fitted by the expression $\frac{S}{S+1} p_{max}$, where $S = P/P_{sat}$ is the saturation parameter, P_{sat} is the saturation power, and p_{max} is the maximum detection probability. The second set is modeled by the expression $\Delta\nu_0\sqrt{1+S}$, where $\Delta\nu_0$ is the linewidth at zero power. The data are reported in the bottom panel of Fig. 3(c), and from a fit to these equations, we were able to extract $P_{sat} = 10.7(1)$ pW in the telecom fiber, which corresponds to ~$1.6 \cdot 10^{-3}$ intra-cavity photons per cavity lifetime [31], and $\Delta\nu_0 = 2.20(7)$ MHz. The probability to detect a photon per trial at saturation approaches $p_{max} = 1\%$, corresponding to a probability that an emitted photon is coupled into the fiber of $p_f \approx 4.3\%$ (see Supplement 1).

The non-linear behavior of the detection probability and linewidth for increasing excitation power is a signature of a single emitter, whereby only one excitation is possible at any given time. Another consequence is the emission of single photons, which can be confirmed by the detection of sub-poissonian statistics in the emitted field. This can be gauged by reconstructing the
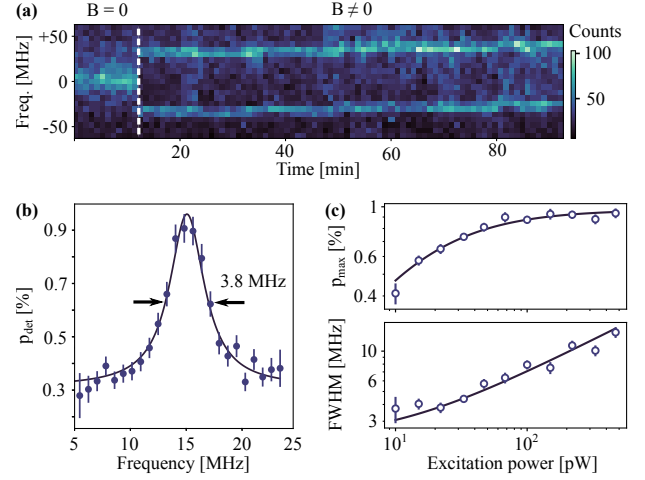
Fig. 3. Single ion analysis. (a) Splitting of the fluorescence excitation spectrum after a magnetic field ($\approx 10^2$ G) is turned on. A limited drift <10 MHz is visible over the course of the measurement. (b) Resonant scan of one of the split lines, obtained for an excitation power of 22 pW in the telecom fiber, showing a FWHM of 3.8 MHz. (c) Saturation scans for linewidth and maximum count rate of a single spectral feature. Both feature a non-linear behavior, typical of two-level systems. The solid lines are fits to the expected function, which give a saturation power of 10.7(1) pW.

second-order correlation function $g^{(2)}(\tau)$ of the emitted field, also called auto-correlation. The $g^{(2)}(\tau)$ of the field emitted by a single ion should feature a dip to zero at $\tau = 0$, presenting at the same time sub-poissonian features and antibunching, both signatures of non-classical light. Any variation from this ideal value comes from the detection of spurious photons, due, for example, to the excitation of neighboring ions, or from the detector dark counts. We measured the $g^{(2)}(\tau)$ by using only one detector and measuring the number of photons detected per excitation trial. This was possible due to the low dead-time of our superconducting detectors (50 ns) compared with the temporal length of the photons (350 μs). By correlating these detection events, we were able to reconstruct a $g^{(2)}(\tau)$ shown in Fig. 4. The data are not background subtracted. The value of $g^{(2)}(0) = 0.24(5)$ is well below the 0.5 threshold for single photon emitters and is compatible with the expected value
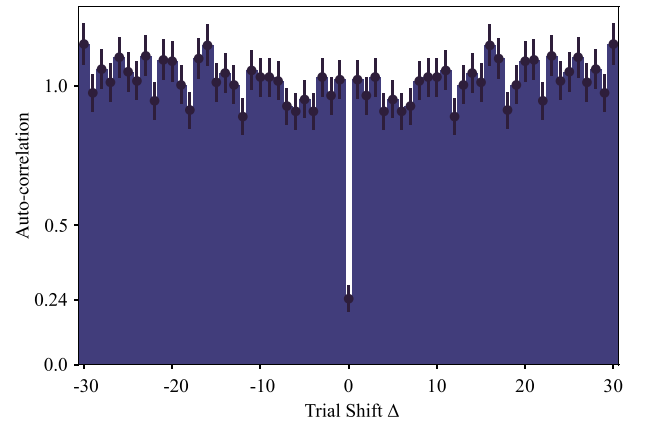
Fig. 4. Autocorrelation function of the light collected from the cavity, showing a clear antibunching dip at zero delay, with a value of 0.24(5). The data are not corrected, and the value at zero delay is compatible with the observed signal-to-noise ratio arising from the dark counts of the detectors. These were set to a detection efficiency of 50%, to reach a dark count rate of 1.4 Hz.

of a perfect single emitter given the noise counts of our detectors, providing conclusive proof of the detection of a single erbium ion in a nanoparticle.

4. DISCUSSION

Our results represent the first demonstration that a single rare-earth ion can be addressed and detected within a nanoparticle coupled to a fiber-microcavity. In our experiments, hundreds of ions were confined to a volume two orders of magnitude smaller than previous realizations, which, due to the careful adjustment of the dielectric mirror coating, were all placed at an anti-node of the cavity electric field. This strongly increases the probability to find ions within a distance that allows strong dipolar interaction. Our platform therefore may open prospects for the realization of quantum processors with hundreds of qubits in a nanoscale volume, which can be efficiently coupled to single photons for quantum networking. Moreover, the erbium ions detected in this work emit single photons at telecommunication wavelength in a fiber-optic setup and could therefore serve as communication qubits. Our approach also enables the coupling of many spectrally separated ions to the cavity, opening the door to frequency multiplexed quantum nodes [35,36].

There are still several challenges ahead towards these goals. The first enabling step will be the realization and full characterization of single qubit gates. Building upon this, the realization of dipolar ion–ion gates requires long spin coherence times as well as a limited and controllable interaction between neighboring ion spins. While narrow optical linewidths have been achieved for Er [20,40], spin–spin interactions at high densities would still limit the spin coherence and the fidelity of the quantum gates. Moreover, the anisotropic g-factor of erbium ions prevents the use of dynamical decoupling techniques [53] to limit the effect of Er–Er interactions. However, this interaction could be heavily reduced by employing the nuclear spins of ^{167}Er combined with strong magnetic fields to freeze out electronic spins, as evidenced by the spin coherence times of 1.3 s that have been measured using these techniques [21], at the cost of a more complicated energy level scheme. Another possibility would be to use non-Kramers ions with long spin coherence times such as europium [25,26] or praseodymium [27], where the spin–spin interaction is strongly reduced and temperature requirements are less strict. For the latter approach, erbium ions could serve as communication qubits to connect quantum processors, taking advantage of the possibility to co-dope the nanoparticles with several ion species [22].

A second challenge is to reach the emission of coherent transform-limited photons from erbium ions to enable the connection of distant nodes via photonic interference. This requires improvements in both the Purcell enhancement and optical coherence time. The former could be significantly increased by improving the finesse and stability of the cavity. The latter is likely limited by the temperature (>6 K) of the sample, which the measured linewidth is consistent with [46], so this could be increased by lowering the operating temperature using a more sophisticated cryostat. Optical homogeneous linewidths of 580 Hz have been achieved recently in Er : Y_2O_3 ceramics at millikelvin temperature [20], and while coherence times in nanoparticles are shorter than in ceramics, significant improvement can be expected [9]. An additional benefit of longer coherence times would be the ability to perform coherent excitation and spin initialization, which will

readily increase by a factor of four the probability to generate a photon per trial.

Another parameter that can be improved is the generation and detection efficiency. The probability to couple an emitted photon in the fiber is currently limited by the mode matching between the cavity mode and the fiber, and by intracavity losses due to scattering from the nanoparticles. The former could be improved using fiber cavities with integrated mode matching optics [54], while the latter could be reduced by embedding the nanoparticles, e.g., in a thin layer of Y_2O_3.

REFERENCES

1. D. D. Awschalom, R. Hanson, J. Wrachtrup, *et al.*, "Quantum technologies with optically interfaced solid-state spins," Nat. Photonics **12**, 516–527 (2018).
2. D. Hucul, I. V. Inlek, G. Vittorini, *et al.*, "Modular entanglement of atomic qubits using photons and phonons," Nat. Phys. **11**, 37–42 (2015).
3. V. Krutyanskiy, M. Meraner, J. Schupp, *et al.*, "Light-matter entanglement over 50 km of optical fibre," npj Quantum Inf. **5**, 72 (2019).
4. T. van Leent, M. Bock, F. Fertig, *et al.*, "Entangling single atoms over 33 km telecom fibre," Nature **607**, 69–73 (2022).
5. A. Javadi, D. Ding, M. H. Appel, *et al.*, "Spin-photon interface and spin-controlled photon switching in a nanobeam waveguide," Nat. Nanotechnol. **13**, 398–403 (2018).
6. C. E. Bradley, J. Randall, M. H. Abobeih, *et al.*, "A ten-qubit solid-state spin register with quantum memory up to one minute," Phys. Rev. X **9**, 31045 (2019).
7. A. Tchebotareva, S. L. Hermans, P. C. Humphreys, *et al.*, "Entanglement between a diamond spin qubit and a photonic time-bin qubit at telecom wavelength," Phys. Rev. Lett. **123**, 063601 (2019).
8. M. Pelton, "Modified spontaneous emission in nanophotonic structures," Nat. Photonics **9**, 427–435 (2015).
9. T. Zhong and P. Goldner, "Emerging rare-earth doped material platforms for quantum nanophotonics," Nanophotonics **8**, 2003–2015 (2019).
10. K. J. Vahala, "Optical microcavities," Nature **424**, 839–846 (2003).
11. E. M. Purcell, "Spontaneous emission probabilities at radio frequencies," Phys. Rev. **69**, 674 (1946).
12. R. M. Macfarlane, "High-resolution laser spectroscopy of rare-earth doped insulators: a personal perspective," J. Lumin. **100**, 1–20 (2002).
13. H. de Riedmatten, M. Afzelius, M. U. Staudt, *et al.*, "A solid-state light-matter interface at the single-photon level," Nature **456**, 773–777 (2008).
14. M. P. Hedges, J. J. Longdell, Y. Li, *et al.*, "Efficient quantum memory for light," Nature **465**, 1052–1056 (2010).

15. J. V. Rakonjac, D. Lago-Rivera, A. Seri, *et al.*, "Entanglement between a telecom photon and an on-demand multimode solid-state quantum memory," Phys. Rev. Lett. **127**, 210502 (2021).

16. A. Ortu, A. Holzäpfel, J. Etesse, *et al.*, "Storage of photonic time-bin qubits for up to 20 ms in a rare-earth doped crystal," npj Quantum Inf. **8**, 29 (2022).

17. N. Sangouard, C. Simon, H. de Riedmatten, *et al.*, "Quantum repeaters based on atomic ensembles and linear optics," Rev. Mod. Phys. **83**, 33–80 (2011).

18. D. Lago-Rivera, S. Grandi, J. V. Rakonjac, *et al.*, "Telecom-heralded entanglement between multimode solid-state quantum memories," Nature **594**, 37–40 (2021).

19. X. Liu, J. Hu, Z.-F. Li, *et al.*, "Heralded entanglement distribution between two absorptive quantum memories," Nature **594**, 41–45 (2021).

20. R. Fukumori, Y. Huang, J. Yang, *et al.*, "Subkilohertz optical homogeneous linewidth and dephasing mechanisms in Er^{3+}:Y_2O_3 ceramics," Phys. Rev. B **101**, 214202 (2020).

21. M. Rancic, M. P. Hedges, R. L. Ahlefeldt, *et al.*, "Coherence time of over a second in a telecom-compatible quantum memory storage material," Nat. Phys. **14**, 50–54 (2018).

22. A. Kinos, D. Hunger, R. Kolesov, *et al.*, "Roadmap for rare-earth quantum computing," arXiv, arXiv:2103.15743 (2021).

23. A. Kinos, L. Rippe, S. Kröll, "Designing gate operations for single-ion quantum computing in rare-earth-ion-doped crystals," Phys. Rev. A **104**, 052624 (2021).

24. A. Kinos, L. Rippe, D. Serrano, *et al.*, "High-connectivity quantum processor nodes using single-ion qubits in rare-earth-ion-doped crystals," Phys. Rev. A **105**, 032603 (2022).

25. B. Casabone, J. Benedikter, T. Hümmer, *et al.*, "Cavity-enhanced spectroscopy of a few-ion ensemble in Eu^{3+}:Y_2O_3," New J. Phys. **20**, 095006 (2018).

26. D. Serrano, J. Karlsson, A. Fossati, *et al.*, "All-optical control of long-lived nuclear spins in rare-earth doped nanoparticles," Nat. Commun. **9**, 2127 (2018).

27. D. Serrano, C. Deshmukh, S. Liu, *et al.*, "Coherent optical and spin spectroscopy of nanoscale Pr^{3+}:Y_2O_3," Phys. Rev. B **100**, 144304 (2019).

28. F. K. Asadi, N. Lauk, S. Wein, *et al.*, "Quantum repeaters with individual rare-earth ions at telecommunication wavelengths," Quantum **2**, 93 (2018).

29. R. Kolesov, K. Xia, R. Reuter, *et al.*, "Optical detection of a single rare-earth ion in a crystal," Nat. Commun. **3**, 1029 (2012).

30. T. Utikal, E. Eichhammer, L. Petersen, *et al.*, "Spectroscopic detection and state preparation of a single praseodymium ion in a crystal," Nat. Commun. **5**, 3627 (2014).

31. A. M. Dibos, M. Raha, C. M. Phenicie, *et al.*, "Atomic source of single photons in the telecom band," Phys. Rev. Lett. **120**, 243601 (2018).

32. T. Zhong, J. M. Kindem, J. G. Bartholomew, *et al.*, "Optically addressing single rare-earth ions in a nanophotonic cavity," Phys. Rev. Lett. **121**, 183603 (2018).

33. M. Raha, S. Chen, C. M. Phenicie, *et al.*, "Optical quantum nondemolition measurement of a single rare earth ion qubit," Nat. Commun. **11**, 1605 (2020).

34. J. M. Kindem, A. Ruskuc, J. G. Bartholomew, *et al.*, "Control and single-shot readout of an ion embedded in a nanophotonic cavity," Nature **580**, 201–204 (2020).

35. S. Chen, M. Raha, C. M. Phenicie, *et al.*, "Parallel single-shot measurement and coherent control of solid-state spins below the diffraction limit," Science **370**, 592–595 (2020).

36. A. Ulanowski, B. Merkel, and A. Reiserer, "Spectral multiplexing of telecom emitters with stable transition frequency," Sci. Adv. **8**, eabo4538 (2022).

37. K. Xia, F. Sardi, C. Sauerzapf, *et al.*, "Tunable microcavities coupled to rare-earth quantum emitters," Optica **9**, 445–450 (2022).

38. A. Ruskuc, C.-J. Wu, J. Rochman, *et al.*, "Nuclear spin-wave quantum register for a solid-state qubit," Nature **602**, 408–413 (2022).

39. M. T. Uysal, M. Raha, S. Chen, *et al.*, "Coherent control of a nuclear spin via interactions with a rare-earth ion in the solid state," PRX Quantum **4**, 010323 (2023).

40. S. Ourari, Ł. Dusanowski, S. P. Horvath, *et al.*, "Indistinguishable telecom band photons from a single erbium ion in the solid state," Nature **620**, 977–981 (2023).

41. D. Riedel, I. Söllner, B. J. Shields, *et al.*, "Deterministic enhancement of coherent photon generation from a nitrogen-vacancy center in ultrapure diamond," Phys. Rev. X **7**, 031040 (2017).

42. D. Wang, H. Kelkar, D. Martin-Cano, *et al.*, "Turning a molecule into a coherent two-level quantum system," Nat. Phys. **15**, 483–489 (2019).

43. N. Tomm, A. Javadi, N. O. Antoniadis, *et al.*, "A bright and fast source of coherent single photons," Nat. Nanotechnol. **16**, 399–403 (2021).

44. B. Merkel, A. Ulanowski, and A. Reiserer, "Coherent and Purcell-enhanced emission from erbium dopants in a cryogenic high-Q resonator," Phys. Rev. X **10**, 041025 (2020).

45. B. Casabone, C. Deshmukh, S. Liu, *et al.*, "Dynamic control of Purcell enhanced emission of erbium ions in nanoparticles," Nat. Commun. **12**, 3570 (2021).

46. M. K. Alqedra, C. Deshmukh, S. Liu, *et al.*, "Optical coherence properties of Kramers' rare-earth ions at the nanoscale for quantum applications," Phys. Rev. B **108**, 075107 (2023).

47. J. Benedikter, H. Kaupp, T. Hümmer, *et al.*, "Cavity-enhanced single-photon source based on the silicon-vacancy center in diamond," Phys. Rev. Appl. **7**, 024031 (2017).

48. S. Pazzagli, P. E. Lombardi, D. Martella, *et al.*, "Self-assembled nanocrystals of polycyclic aromatic hydrocarbons show photostable single-photon emission," ACS Nano **12**, 4295–4303 (2018).

49. D. Hunger, T. Steinmetz, Y. Colombe, *et al.*, "A fiber Fabry–Perot cavity with high finesse," New J. Phys. **12**, 065038 (2010).

50. C. Deshmukh, "Detection of a single erbium ion in a nanoparticle," Ph.D. thesis (Universitat Politècnica de Catalunya, 2022).

51. S. Welinski, et al., are preparing a manuscript to be called "High bandwidth, low-spurious optical waveform generator for quantum emitters manipulation and control."

52. R. D. Shannon and C. T. Prewitt, "Effective ionic radii in oxides and fluorides," Acta Crystallogr. Sec. B **25**, 925–946 (1969).

53. B. Merkel, P. Cova Fariña, and A. Reiserer, "Dynamical decoupling of spin ensembles with strong anisotropic interactions," Phys. Rev. Lett. **127**, 030501 (2021).

54. G. K. Gulati, H. Takahashi, N. Podoliak, *et al.*, "Fiber cavities with integrated mode matching optics," Sci. Rep. **7**, 5556 (2017).

55. S. Grandi, "Supporting data for 'Detection of single ions in a nanoparticle coupled to a fiber cavity'," Zenodo (2023), https://doi.org/10.5281/zenodo.8101826.